Controlled neuromodulation naturally interacts with homeostasis to produce robust and modulable neuronal function

Arthur Fyon[1*], Guillaume Drion[1]

1 Department of Electrical Engineering and Computer Science, University of Liège, 10 Allée de la Découverte, Liège, 4000, Belgium

* afyon@uliege.be

Abstract

Neurons rely on two interdependent mechanisms – homeostasis and neuromodulation – to maintain robust and adaptable functionality. Homeostasis stabilizes neuronal activity by adjusting ionic conductances, whereas neuromodulation dynamically modifies ionic properties in response to external signals carried by neuromodulators. Combining these mechanisms in conductance-based models often produces unreliable outcomes, particularly when sharp neuromodulation interferes with homeostatic tuning. This study explores how a biologically inspired neuromodulation controller can harmonize with homeostasis to ensure reliable neuronal function. Using computational models of stomatogastric ganglion and dopaminergic neurons, we demonstrate that controlled neuromodulation preserves neuronal firing patterns while homeostasis simultaneously maintains target intracellular calcium levels. Unlike sharp neuromodulation, the neuromodulation controller integrates activity-dependent feedback through mechanisms mimicking G-protein-coupled receptor cascades. The interaction between these controllers critically depends on the existence of an intersection in conductance space, representing a balance between target calcium levels and neuromodulated firing patterns. Maximizing neuronal degeneracy enhances the likelihood of such intersections, enabling robust modulation and compensation for channel blockades. We further show that this controller pairing extends to network-level activity, reliably modulating central

pattern generators rhythmic activity. This study highlights the complementary roles of homeostasis and neuromodulation, proposing a unified control framework for maintaining robust and adaptive neural activity under physiological and pathological conditions.

Author summary

Neurons must maintain stable activity while adapting to changing demands, relying on two mechanisms: homeostasis, which stabilizes activity, and neuromodulation, which adjusts behavior to external signals. These mechanisms often interact, but their improper coordination can lead to dysfunction. This study uses computational models to show how controlled neuromodulation – mimicking biological feedback – can be harmonized with controlled homeostasis to ensure robust neuronal function. The system compensates for channel blockades and maintains critical activity patterns for both single neurons and networks even when faced with neuronal parameter variability. These insights not only deepen our understanding of neural robustness, but also suggest safer pharmacological strategies targeting neuromodulatory pathways, offering potential breakthroughs in treating neurological disorders without disrupting essential cellular mechanisms.

Introduction

Brain activity is continuously shaped by neuromodulators and neuropeptides, including dopamine, serotonin, and histamine [1, 2]. Neuromodulators dynamically influence single-neuron activity, input-output properties, and synaptic strength, enabling neuronal networks to adapt to changing needs, contexts, and environments [3–5]. This modulation occurs through the regulation of transmembrane proteins, such as ion channels and receptors, which alters neuronal excitability and synaptic dynamics [6, 7]. While experimental studies highlight the ubiquity of neuromodulation, the fundamental principles governing its effects remain incompletely understood, making computational approaches crucial for unraveling its mechanisms.

Neuromodulation coexists with homeostatic plasticity, a process that gradually

adjusts neuronal membrane properties to maintain a target activity level [8–14]. Neuronal cells are dependent on homeostatic mechanisms to maintain optimal functionality throughout the extended useful life of mammals [15]. Despite continuous turnover of transmembrane proteins, such as ion channels and receptors, occurring on varying temporal scales ranging from hours to weeks [16], the robustness and excitability of neurons must remain undisturbed [17]. Among homeostatic mechanisms, intrinsic homeostatic plasticity adjusts ion channel conductances in response to intracellular calcium levels [18, 19]. However, since both neuromodulation and homeostasis act on the same targets (ion channels) and may have competing objectives, understanding their interaction is essential [2, 17].

We propose to study the interaction between neuromodulation and homeostasis using conductance-based models. These models provide a biophysically accurate representation of neuronal dynamics by describing the electrical properties of the neuronal membrane. The membrane is modeled as an RC circuit, while ion channels are represented as nonlinear conductances that evolve according to experimentally derived activation and inactivation kinetics [20]. Conductance-based models remain the most faithful mathematical representations of biological neurons, as they allow for the direct incorporation of ion channel dynamics extracted from experimental data, following the methodology first introduced by Hodgkin and Huxley [21]. Over the years, numerous conductance-based models have been developed to describe a variety of neuronal cell types across different species and brain regions [22–28]. This study focuses on a conductance-based model of stomatogastric ganglion (STG) neurons [22]. STG neurons are key components of rhythmic circuits that generate motor patterns driving stomach muscle contractions in crustaceans. This model was chosen for its ability to reproduce diverse firing patterns – ranging from tonic spiking to bursting – and its rich set of ion channels, which enable degeneracy. Specifically, the model includes classical fast sodium and delayed rectifier potassium channels, A-type and calcium-activated potassium channels, T-type and slow calcium channels, as well as hyperpolarization-activated H-channels.

We model intrinsic homeostasis by using the homeostatic controller proposed by [29], which adjusts all ionic conductances up or down based on the neuron average intracellular calcium level. If the calcium level is lower than a target reference value, the

controller increases ionic conductances according to homeostatic tuning rules, and conversely, decreases them if the calcium level is above the target. Importantly, these rules ensure that conductances are tuned along a single axis, preserving their relative ratios and maintaining correlations between them. This self-tuning mechanism allows neurons to counteract perturbations while preserving stable activity.

Neuromodulation is modeled using two different approaches. On the one hand, we model neuromodulation as an acute change in target conductance values leading to a desired neuromodulated state in degenerate populations, which we call "sharp neuromodulation". On the other hand, we implement the neuromodulation controller developed by [30], which is designed to enable robust modulation of neuronal activity. We call this approach "controlled neuromodulation". One of its key properties is that it accounts for neuronal degeneracy, meaning that neurons with different ion channel compositions but similar activity patterns respond in a consistent manner to neuromodulation [31]. This feature is particularly important because biological neuronal populations exhibit significant variability in their underlying conductance parameters while maintaining functional stability. By leveraging degeneracy, the neuromodulation controller can apply the same control signal across a population of neurons with diverse conductance profiles, ensuring reliable and predictable neuromodulation.

We first investigate the interaction between intrinsic homeostatic plasticity and neuromodulation at the single-neuron level and show that combining intrinsic homeostasis with either sharp or controlled neuromodulation leads to vastly different outcomes. Secondly, we provide a mechanistic explanation for these different outcomes. We then extend our analysis to rhythmic neuronal networks, where neuromodulation plays a critical role in adjusting oscillatory patterns. By carefully integrating homeostatic and neuromodulatory control mechanisms, we aim to develop a unified framework that combines the strengths of both approaches. This integrated controller enables robust modulation of neuronal activity while ensuring long-term stability, shedding light on how neuromodulation and homeostasis coexist in biological systems.

Results

Interference between homeostasis and sharp neuromodulation leads to pathological outcomes

We first examine the interplay between a state-of-the-art model of cellular homeostasis [29] and sharp neuromodulation [32]. Here, *sharp neuromodulation* is defined as a direct, externally driven modification of a subset of ion channel maximal conductances, resulting in a change in neuronal spiking behavior. We specifically focus on a robust transition from tonic spiking to bursting in degenerate neuronal populations, *i.e.* populations composed of neurons that exhibit similar firing behaviors despite differences in underlying conductance profiles.

To explore this interaction, we applied sharp neuromodulation to a population of degenerate neurons generated using the dataset from [32] (Fig 1). Sharp neuromodulation consisted of directly modifying the maximal conductances of A-type potassium ($\bar{g}_{\mathrm{A}}$) and slow calcium ($\bar{g}_{\mathrm{CaS}}$) channels to transition neurons from tonic spiking to bursting. We then allowed homeostatic compensation to unfold. Since bursting increases overall neuronal activity, intracellular calcium levels rise, triggering a decrease in all conductances according to homeostatic tuning rules. Three representative conductance trajectories ($N = 200$) are shown in Fig 1 (top), while Fig 1 (bottom) illustrates calcium dynamics across the population (note that to facilitate observation of both mechanisms within a single trace, the homeostatic controller was accelerated compared to its original implementation). Despite initially similar firing patterns and a similar outcome of sharp neuromodulation, homeostatic compensation produced highly variable and often unreliable outcomes in terms of modulated activity, while still regulating intracellular calcium. Depending on the initial conductance state, neuromodulation led to new states where homeostasis could either maintain functional activity, result in pathological behavior, or drive neurons into unphysiological regimes. This finding underscores a fundamental property of degeneracy: neurons with different underlying conductances can exhibit similar activity yet respond differently to perturbations, such as neuromodulation.

To understand the source of this unreliability, it is necessary to examine both

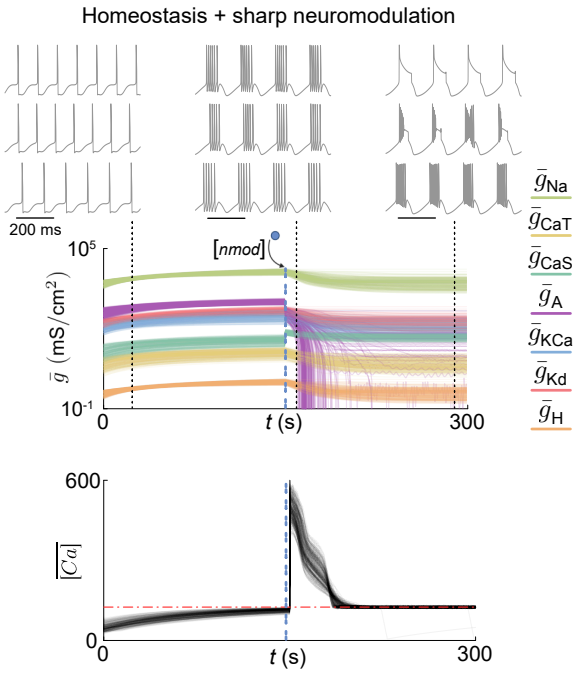

Fig 1. Interference between homeostasis and sharp neuromodulation leads to pathological outcomes. Time evolution of all conductances in the STG model, displayed on a logarithmic scale, during homeostasis with sharp neuromodulation (instantaneous changes in $\bar{g}_{\mathrm{CaS}}$ and $\bar{g}_{\mathrm{A}}$ starting at the dashed blue line) for a degenerate population of 200 models (top). The corresponding mean intracellular calcium concentration over time (bottom) shows the target value (red dash-dotted line) is maintained both before and after sharp neuromodulation.

mechanisms in more detail. The homeostatic model [29] relies on intracellular calcium as a feedback signal. The neuron continuously averages its intracellular calcium level over time and adjusts conductances accordingly: if calcium falls below a target level (red dash-dotted line in Fig 1 bottom), ion channel transcription and translation increase, raising all conductance values, and vice versa. This phenomenon happens on a relatively slow timescale, which can last up to days [18]. In contrast, sharp neuromodulation, implemented using the method from [32], directly modifies a subset of ion channel conductances, which upsets the homeostasis setpoint, defined by the intracellular calcium target level. As homeostasis kicks in to recover its calcium set point, there are no guarantees that the neuromodulated function is maintained as ion channel conductances are modified, which often leads to pathological or unphysiological outcomes.

This type of interference was anticipated in [29], where the authors demonstrated

that homeostatic regulation can produce diverse responses to perturbations such as ion channel deletions. Depending on the initial conditions, a deletion may either preserve function, disrupt it, or lead to pathological compensation. Our results extend this idea by showing that even physiological disturbances, such as neuromodulation, can induce similar unpredictability when coupled with homeostatic regulation.

Controlled neuromodulation and homeostasis naturally lead to robust and modulable neuronal function

In biological systems, neuromodulation occurs through an intracellular cascade that indirectly links changes in neuromodulation concentration and changes in targeted conductance values using an intermediate signal such as *e.g.* cyclic amp. We have recently shown that this indirect action of neuromodulation on conductance values could be viewed as an intracellular controller (Fig 2A, top), which largely improves reliability of neuromodulatory action on highly degenerate populations [30]. We call this mechanism "controlled neuromodulation" to contrast with the sharp neuromodulation described above. Unlike sharp neuromodulation, which imposes instantaneous conductance changes, the neuromodulation controller provides continuous and adaptive modulation, ensuring stable functional transitions.

Using the same protocol as for sharp neuromodulation, we now study the interaction between controlled neuromodulation and homeostasis. Fig 2B illustrates the transition from tonic spiking to bursting in a degenerate population of STG neuron models, identical to those in Fig 1, but when using controlled neuromodulation instead of sharp neuromodulation. Initially, all neurons exhibit tonic firing, with homeostasis tuning conductances along a tonic spiking homogeneous scaling line to maintain a target calcium level. Midway through the simulation, controlled neuromodulation is applied, gradually adjusting $\bar{g}_{\mathrm{CaS}}$ and $\bar{g}_{\mathrm{A}}$ to induce bursting. As in the case of sharp neuromodulation, this transition increases intracellular calcium levels, leading to an adaptive shift in conductance values. Homeostatic regulation then readjusts overall conductance magnitudes, but here the interaction between homeostasis and controller neuromodulation ensures that the newly established neuromodulated state is maintained. Ultimately, the population reaches a stable configuration where both the

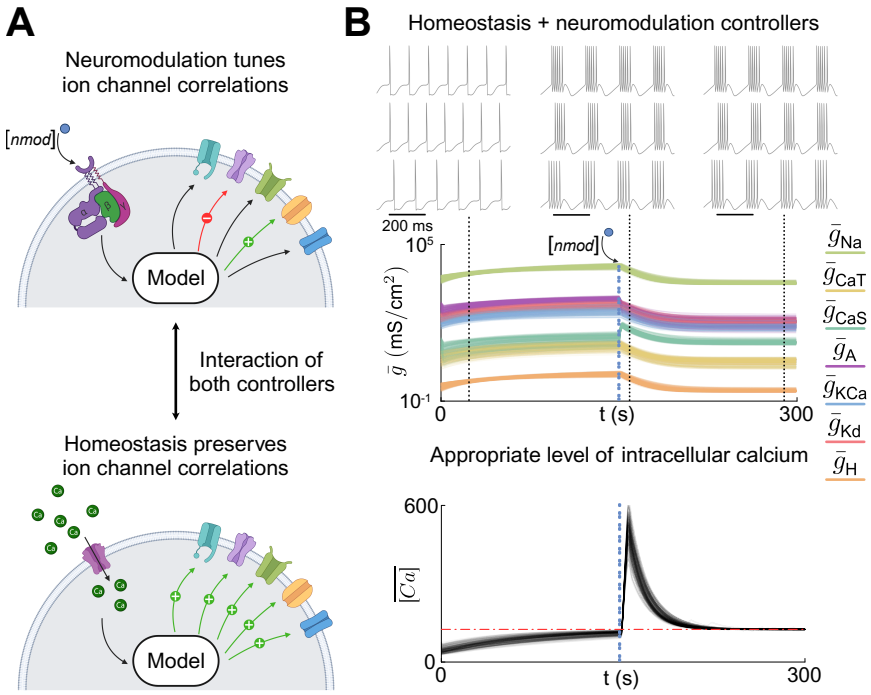

Fig 2. Controlled neuromodulation and homeostasis naturally lead to robust and modulable neuronal function.
A. Schematic representation of neuromodulation (left) and homeostasis (right) cascades. Neuromodulators bind to G-protein receptors, triggering complex signaling pathways that selectively affect subsets of ion channels. In contrast, homeostasis senses intracellular calcium levels and regulates them by adjusting all conductances uniformly. **B.** Time evolution of all conductances in the STG model, displayed on a logarithmic scale, during homeostasis with controlled neuromodulation (controlled changes in $\bar{g}_{\mathrm{CaS}}$ and $\bar{g}_{\mathrm{A}}$) for a degenerate population of 200 models (left). The corresponding mean intracellular calcium concentration over time (right) shows the target value (red dash-dotted line) is maintained both before and after controlled neuromodulation.

neuromodulated function and intracellular calcium homeostasis are fulfilled.

To demonstrate the generality of this approach, we applied the same framework to a midbrain dopaminergic neuron model adapted from [23] (see Supporting Information, S1 Appendix). As in the STG model, a transition from tonic spiking (pacemaking) to strong bursting was induced by modulating N-type and L-type calcium conductances ($\bar{g}_{\mathrm{CaN}}$ and $\bar{g}_{\mathrm{CaL}}$) through controlled neuromodulation. Homeostatic compensation continuously regulated calcium levels, ensuring a reliable and robust outcome despite initial conductance degeneracy within the neuronal population.

Controlled neuromodulation tunes the direction of homeostasis-driven changes in conductance values to ensure stable neuromodulated function during homeostatic regulation

To study the mechanisms underlying the constructive interaction between controlled neuromodulation and homeostasis, we plot the conductance trajectories of the simulations from Fig 1 in the plane of modulated conductances, $\bar{g}_{\mathrm{CaS}}$ and $\bar{g}_{\mathrm{A}}$, during tonic spiking homeostatic compensation for both sharp and controlled neuromodulation (Fig 3A). Initially, as calcium levels remain below the threshold, homeostasis increases the modulated conductances along a homogeneous scaling direction characteristic of tonic spiking. This direction corresponds to a line intersecting the origin, with variability due to conductance degeneracy within the population, and its slope is determined by the relative time constants of mRNA transcription in the homeostasis model, with steady-state analysis predicting $\bar{g}_i/\bar{g}_j \approx \tau_{m_j}/\tau_{m_i}$ [29]. When neuromodulation is applied, all conductances are adjusted to reshape their ratios and induce bursting (Fig 3B). Importantly, neuromodulatory actions follow the same direction across neurons but vary in magnitude depending on individual neuronal states [32]. This modulation leads to a sharp increase in intracellular calcium levels. Once neuromodulation ceases, the long-term outcome depends on the type of neuromodulation applied (Fig 3C).

Under sharp neuromodulation, homeostasis operates alone in the bursting phase, following the scaling direction characteristic of its reference, *i.e.* unmodulated, state set by the relative time constants of mRNA transcription in the homeostasis model (Fig 3C, left). This results in a decrease in calcium levels, but as shown in Fig 1, the response is unreliable and often undesirable. Specifically, for most neurons, the homeostatic controller reduces $\bar{g}_{\mathrm{A}}$ toward negative values (saturated at 0 to prevent model instability) to compensate for $\bar{g}_{\mathrm{CaS}}$, driving the neuron away from robust bursting and leading to heterogeneous activity changes across the population.

In contrast, controlled neuromodulation allows the homeostatic and neuromodulation controllers to act together, maintaining the new conductance ratios associated with bursting (Fig 3C, right). As a result, homeostatic regulation follows a new homogeneous scaling trajectory aligned with bursting conductance ratios. These

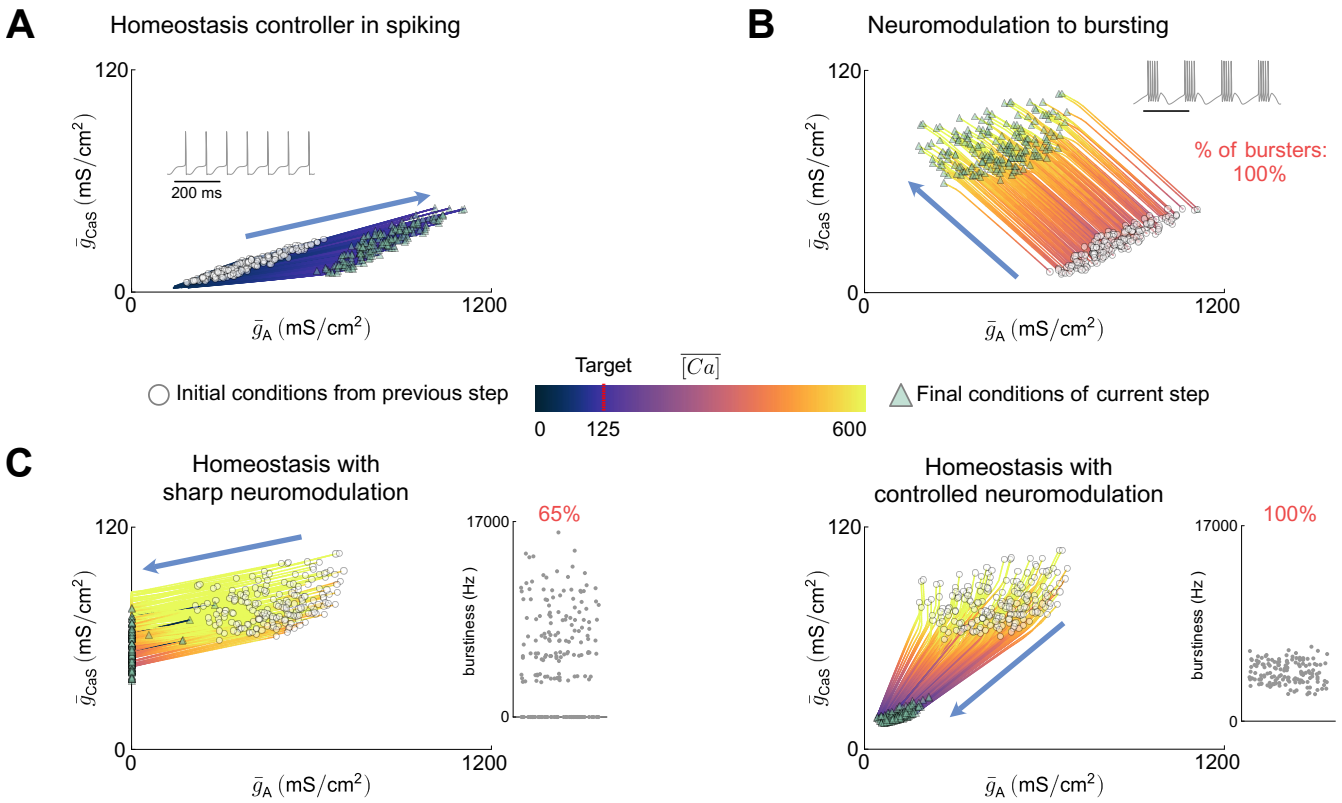

Fig 3. Controlled neuromodulation tunes the direction of homeostasis-driven changes in conductance values to ensure stable neuromodulated function during homeostatic regulation.
A. Trajectories of the STG population from Fig 1 in the modulated conductance space during homogeneous scaling in tonic spiking only. As expected from homeostasis, all neurons move in the same direction. White circles represent the initial conditions at the start of the step, and the green triangle marks the final conditions.
B. Same as panel A, but during the brief period when neuromodulation is active. All trajectories are parallel to one another.
C. Same as panels A and B, but during the homeostasis phase following neuromodulation. The outcome depends on the type of neuromodulation: sharp (left) or controlled (right). Sharp neuromodulation results in non-robust outcomes, whereas controlled neuromodulation preserves robust neural function.

trajectories converge toward the origin, as in tonic spiking, but with a distinct direction determined by neuromodulation. Due to initial conductance degeneracy, the exact scaling varies across the population. The shift between the two homogeneous scalings – tonic spiking and bursting – emerges from neuromodulation, ensuring that the desired neuromodulated function is maintained.

The incompatibility of sharp neuromodulation with homeostasis can be further analyzed using a schematic representation of the modulated conductance plane (Fig 4A). In this plane, different combinations of $\bar{g}_{\mathrm{CaS}}$ and $\bar{g}_{\mathrm{A}}$ can yield similar calcium levels, forming calcium isoclines (green dashed lines). Similarly, different conductance values

can result in similar firing activity, forming activity isoclines (blue dashed lines). While calcium isoclines are parallel, activity isoclines radiate from the origin and rotate around it. This organization reflects homeostatic tuning rules: different conductance ratios correspond to distinct firing modes [29]. Initially, the neuron operates at the intersection of a target spiking isocline and a target calcium isocline. When sharp neuromodulation is applied, conductances shift to a new state corresponding to strong bursting, moving the neuron to a higher calcium isocline. Homeostasis then acts to restore calcium levels, but because it retains the "native" tonic spiking scaling direction, it alters conductances along the spiking isocline rather than preserving the newly induced bursting state. As a result, the neuron drifts away from the bursting isocline, potentially disrupting its function. This explains why sharp neuromodulation leads to unreliable outcomes when coupled with homeostasis.

To reconcile homeostasis and neuromodulation and achieve robust functional modulation, we leverage their distinct timescales. Neuromodulation controls specific ionic conductances, while homeostasis adjusts all conductances over a slower timescale to regulate calcium levels. In the modulated conductance plane (Fig 4B), the neuron initially follows the same trajectory as in Fig 4A. However, under controlled neuromodulation, both controllers remain active. When homeostasis lowers calcium levels and shifts the neuron away from the bursting isocline, the neuromodulatory controller counteracts this deviation, bringing the neuron back toward the bursting isocline and preserving the desired function. Because the neuromodulatory controller operates orders of magnitude faster than the homeostatic controller, its rapid corrections render homeostatic perturbations negligible. This interaction constrains changes in conductance ratios along the target activity isocline (strong bursting in this case). Ultimately, the neuron stabilizes at the intersection of the target calcium and target activity isoclines, where both controllers achieve their objectives.

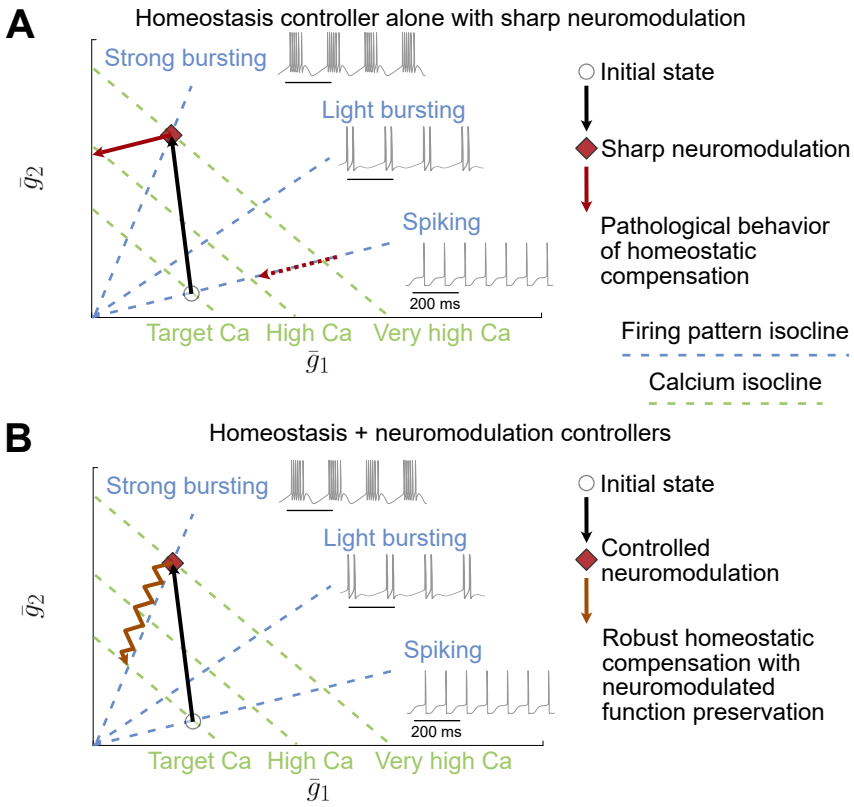

Fig 4. Schematic explanation of why controlled neuromodulation integrates better with homeostasis compared to sharp neuromodulation.
A. Schematic of the modulated conductance space for homeostasis combined with sharp neuromodulation. Initially (white circles), the neuron spikes at the target calcium level, located at the intersection of the firing pattern isocline (dashed blue lines) and the calcium level isocline (dashed green lines). Following sharp neuromodulation to a new firing pattern (red diamond), calcium levels sharply increase. Homeostasis reduces calcium (solid red arrow) by moving along the same direction as before neuromodulation (dashed red arrow), causing the neuron to deviate from the neuromodulated firing pattern isocline.
B. Same as panel A, but with controlled neuromodulation. The initial steps are identical, but after neuromodulation, as homeostasis acts to reduce calcium, controlled neuromodulation simultaneously adjusts to keep the neuron on the neuromodulated firing pattern isocline (sawtooth red arrow). Because controlled neuromodulation operates on a much faster timescale than homeostasis, the neuron remains on the neuromodulated firing pattern isocline throughout.

Controlled neuromodulation and homeostasis ensure the preservation of function under physiologically recoverable disturbances

By employing this tandem of controllers, neuronal function becomes robust to channel blockade, provided that the channel deletion is compensable. While homeostasis alone

may lead to unreliable recovery, incorporating controlled neuromodulation stabilizes the neuronal response to blockade, even in highly degenerate neuronal populations. Furthermore, if the blocked channel function can be physiologically recovered – meaning other channels can substitute for its role – there exists an optimal combination of neuronal feedback gains that preserves the function. In essence, when a channel is blocked, a specific concentration of neuromodulators can maintain the function.

For example, in Fig 5, various channel blockades are applied to a degenerate population of STG conductance-based models equipped with the combined homeostasis/neuromodulation tandem. The target behavior of the population is regular bursting. In Fig 5A, H-type channels are blocked. Here, the function remains intact even immediately after the blockade, without requiring compensation. The combined action of homeostasis and controlled neuromodulation then ensures that intracellular calcium levels are restored on a population-wide scale, maintaining the function.

In Fig 5B and C, T-type calcium and calcium-activated potassium channels are blocked, respectively. In these cases, the blockade largely disrupts bursting. However, allowing the homeostasis/neuromodulation controllers to compensate restores function in most neurons, albeit with some displaying irregular bursting. Additionally, intracellular calcium levels stabilize at their target values. This recovery is possible because the actions of H-type, T-type calcium, and calcium-activated potassium channels are degenerate, allowing their function to be compensated by other channels in the cell. The STG neuron model includes numerous channels operating on slow and ultraslow timescales, enabling compensation over these timescales. Notably, only the loss of the calcium-activated potassium channel has been compensated by adjusting neuronal feedback gains – equivalent to modifying neuromodulator concentrations – as in control conditions.

In contrast, the blockade of fast transient sodium channels is irrecoverable (Fig 5D), as these channels are essential for spike initiation on a fast timescale. Once the blockade is applied, compensation cannot restore spiking because sodium channel function is non-degenerate and operates on a timescale that alternative channels cannot compensate for. Consequently, intracellular calcium levels also fail to reach their target values. A similar outcome would occur following the blockade of delayed rectifier potassium channels, which are responsible for the downstroke of spikes.

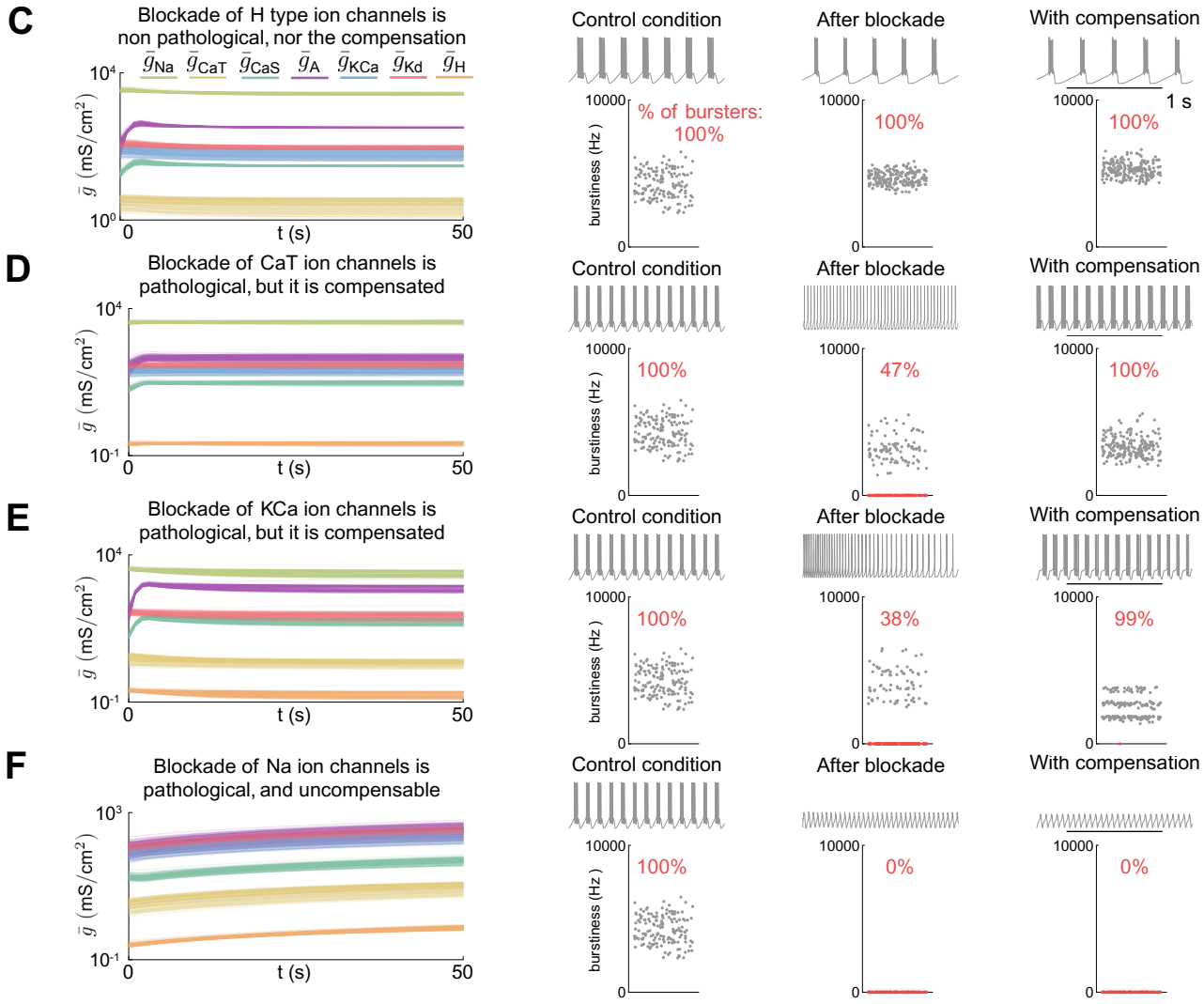

Fig 5. Controlled neuromodulation and homeostasis ensure the preservation of function under physiologically recoverable disturbances.
A. Time evolution of all conductances in the STG model, displayed on a logarithmic scale, during homeostasis with controlled neuromodulation (controlled changes in $\bar{g}_{\mathrm{CaS}}$ and $\bar{g}_{\mathrm{A}}$ starting at the dashed blue line) for a degenerate population of 200 models with H-type ion channel blockade (left). The corresponding distribution of behaviors before the blockade, immediately after the blockade, and following compensation (right) demonstrates the effect of the blockade. In this case, no neurons lose bursting due to the channel blockade or compensation.
B. Same as panel A, but with a CaT channel blockade. The blockade causes half of the neurons to lose bursting; however, all neurons recover bursting with compensation.
C. Same as panel A, but with a KCa channel blockade. The blockade causes more than half of the neurons to lose bursting, but nearly all recover bursting with compensation.
D. Same as panel A, but with a Na channel blockade. The blockade causes all neurons to lose bursting, and compensation does not restore bursting due to the non-degenerate essential role of Na channels.

Central pattern generator networks can be robustly modulated to orchestrate their rhythmic output

The application of this tandem of controllers extends beyond single neurons to networks, particularly central pattern generators (CPGs). CPGs are self-organized neuronal

circuits composed primarily of bursting neurons connected through inhibitory synapses, capable of generating rhythmic output without external input [33, 34]. A well-studied example is the circuit responsible for the pyloric and gastric mill rhythms in crustaceans, located in the stomatogastric ganglion. This network produces two distinct rhythms: the fast pyloric rhythm and the slow gastric mill rhythm. These rhythmic outputs are essential for coordinating muscle contractions in the stomach for digestion, among other functions. A minimal network model of such a bi-rhythmic circuit is investigated in Fig 6 [35, 36]. It consists of two half-center oscillators operating at different speeds, connected via a central neuron. Half-center oscillators are formed by two bursting neurons connected through mutual inhibition, allowing them to fire anti-phase bursts. In this model, the purple and blue neurons constitute the fast half-center oscillator (representing the pyloric rhythm), while the green and yellow neurons form the slow half-center oscillator (representing the gastric mill rhythm). The red neuron acts as the central element, also in bursting mode. It has been shown that the gastric mill rhythm requires neuromodulatory input to be activated [37].

In this study, the tandem of controllers reliably induces the gastric mill rhythm, whereas homeostasis combined with sharp neuromodulation does not. Under control conditions (Fig 6A), *i.e.*, in the absence of neuromodulatory input to the gastric mill rhythm, only the pyloric rhythm remains active, with the central neuron bursting continuously. Notably, conductance variability is observed within the network (Fig 6A right). When neurons are equipped with homeostasis alone, the activation of sharp neuromodulation for the gastric mill rhythm leads to a rapid loss of function due to the unreliability of this combination (Fig 6B middle). However, with controlled neuromodulation, the gastric mill rhythm is successfully induced and sustained (Fig 6B right). Despite the intrinsic degeneracy of the neurons, reflected in significant variability in conductance ratios, the network achieves stable rhythmic output while maintaining appropriate intracellular calcium levels.

This toy experiment demonstrates that the tandem of homeostasis and controlled neuromodulation can be applied in computational models to modulate and sustain not only single-neuron activity but also network-level dynamics.

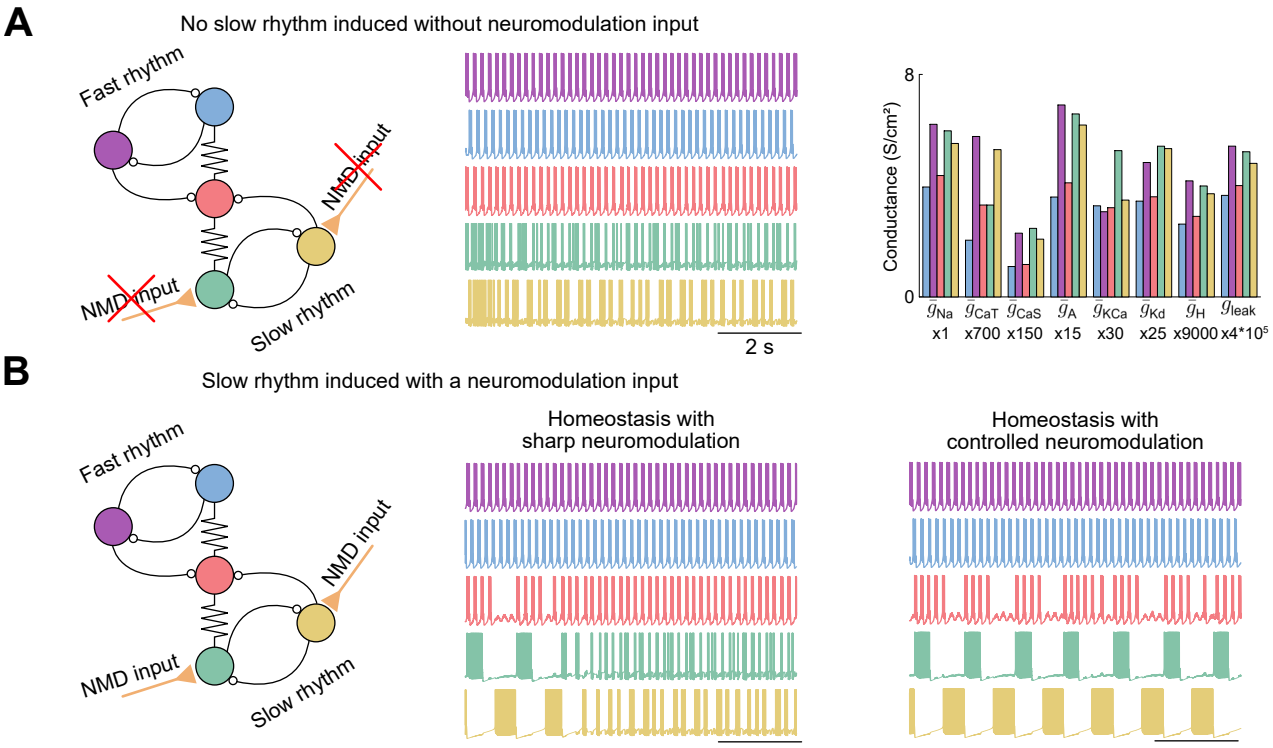

Fig 6. Central pattern generator networks can be robustly modulated to orchestrate their rhythmic output.
A. Control condition of the simplified pyloric/gastric mill rhythm network (left), inspired from [35]. Without neuromodulation, the fast rhythm is active (top two traces, middle), while the slow rhythm is inactive (bottom two traces, middle). In this case, all neurons in the network exhibit degenerate conductances (right).
B. Schematic representation of the activated slow rhythm network (left), modulated by either sharp neuromodulation (middle) or controlled neuromodulation (right). With sharp neuromodulation, the slow rhythm fails due to its unreliability, whereas controlled neuromodulation sustains the slow rhythm.

Discussion

The efficient and robust integration of homeostasis and neuromodulation in neurons remains an open question, with several hypotheses proposed to explain their interaction [2, 38]. Improper integration of these mechanisms – for instance, combining sharp neuromodulation with a homeostatic controller – can lead to negative interactions, resulting in unreliable behaviors or numerical instabilities.

In contrast, pairing a homeostatic controller with controlled neuromodulation enables reliable modulation of neural function while maintaining appropriate calcium levels. This approach is biologically inspired, as neuromodulation is known to be activity-dependent, as observed experimentally [39, 40]. Specifically, the neuromodulation controller models the role of G-protein-coupled receptors and second

messengers, embedding feedback within the metabolic neuromodulation cascade [41, 42]. This reliable interaction extends to neural circuits, such as the gastric mill circuit in crabs, where it contributes to robust network-level function [2].

However, the success of this interaction critically depends on a point in the conductance space where both controllers converge. This point represents a neural activity pattern that supports neuromodulated firing while maintaining homeostatic calcium levels. As shown in Fig 4, it corresponds to the intersection of the strong bursting isocline (the target of controlled neuromodulation) and the homeostatic calcium setpoint. When no such intersection exists – *e.g.*, under sodium channel blockade (Fig 5) – neither neuromodulated activity nor calcium homeostasis can be sustained. This may lead to pathological compensations, where one controller prioritizes calcium regulation at the expense of the target firing pattern [43–45]. Additionally, discontinuities in neuromodulated firing patterns may induce transient pathological behaviors.

Maximizing convergence between these control mechanisms requires increasing the probability of both an intersection and a continuous path in conductance space. We hypothesize that this can be achieved by maximizing neuronal degeneracy [31, 46–49]. Higher degeneracy increases the likelihood that the functional and dynamical role of one ion channel can be compensated by others, thereby preserving both the path and the intersection. This highlights the crucial role of degeneracy in enabling robust, neuromodulated neural function.

Finally, these findings underscore the potential risks associated with pharmacological ion channel blockade [50–52]. If neuronal degeneracy is insufficient, such interventions may compromise the ability to sustain robust neuromodulation. As an alternative, we propose targeting elements within the neuromodulation cascade – such as second messengers or other components of the control loop – as more reliable pharmacological strategies. By preserving the dynamics of controlled neuromodulation, these interventions could offer a more robust alternative to direct ion channel blockade.

Materials and methods

Programming language

The Julia programming language was used in this work [53]. Numerical integration was realized using *DifferentialEquations.jl*.

Conductance-based model

For all experiments, single-compartment conductance-based models were employed. These models articulate an ordinary differential equation for the membrane voltage V, where N ion channels are characterized as nonlinear dynamic conductances, and the phospholipid bilayer is represented as a passive resistor-capacitor circuit. Mathematically, the voltage-current relationship of any conductance-based neuron model is expressed as follows:

$$\begin{aligned} I_C &= C\frac{\mathrm{d}V}{\mathrm{d}t} + g_{\mathrm{leak}}(V - E_{\mathrm{leak}}) = -I_{\mathrm{int}} + I_{\mathrm{ext}}, \\ &= -\sum_{\mathrm{ion}\in\mathcal{I}} g_{\mathrm{ion}}(V,t)(V - E_{\mathrm{ion}}) + I_{\mathrm{ext}}. \end{aligned}$$

Here, C represents the membrane capacitance, g_{ion} denotes the considered ion channel conductance and is non-negative, gated between 0 (all channels closed) and $\bar{g}_{\mathrm{ion}}$ (all channels open), E_{ion} and E_{leak} are the channel reversal potentials, $\mathcal{I}$ is the index set of intrinsic ionic currents considered in the model, and I_{ext} is the current externally applied *in vitro*, or the combination of synaptic currents. Each ion channel conductance is nonlinear and dynamic, represented by $g_{\mathrm{ion}}(V,t) = \bar{g}_{\mathrm{ion}} m_{\mathrm{ion}}^a(V,t) h_{\mathrm{ion}}^b(V,t)$, where m_{ion} and h_{ion} are variables gated between 0 and 1, modeling the opening and closing gates of ion channels, respectively. Throughout this study, the isolated crab STG neuron model of [22] was employed.

The STG model consists of seven ion channels that operate on various time scales: fast sodium channels ($\bar{g}_{\mathrm{Na}}$); delayed-rectifier potassium channels ($\bar{g}_{\mathrm{Kd}}$); T-type calcium channels ($\bar{g}_{\mathrm{CaT}}$); A-type potassium channels ($\bar{g}_{\mathrm{A}}$); slow calcium channels ($\bar{g}_{\mathrm{CaS}}$); calcium controlled potassium channels ($\bar{g}_{\mathrm{KCa}}$); and H channels ($\bar{g}_{\mathrm{H}}$).

The homeostatic controller

The homeostatic controller adjusts all conductances using an integration rule described in [29]. Let $\bar{g}_i$ denote the conductance of ion channel $i \in [1, N]$, and m_i the corresponding mRNA concentration. The dynamics of the homeostatic controller are governed by the following equations:

$$\tau_i \dot{m}_i = [Ca^{+2}]_{\text{target}} - [Ca^{+2}],$$
$$\tau_g \dot{\bar{g}}_i = m_i - \bar{g}_i,$$

where $[Ca^{+2}]$ and $[Ca^{+2}]_{\text{target}}$ represent the calcium level and its target value, respectively. In essence, the calcium level error is integrated into the mRNA levels, which subsequently modulate the corresponding channel conductances. This regulation aims to bring the calcium level to its target value, as higher channel conductances (particularly calcium-conducting ones) facilitate greater calcium influx. Starting from any initial condition, this controller drives the cell along a line in conductance space known as the homogeneous scaling line. This line passes through both the initial condition and the origin of the conductance space axes. Steady-state analysis reveals that the conductance ratios remain invariant, such that $\frac{\bar{g}_i}{\bar{g}_j} = \frac{\tau_j}{\tau_i}$. This invariance ensures that the relative scaling of conductances is preserved during homeostatic compensation. Consequently, the cell conductance properties develop along the homogeneous scaling beam defined by these ratios.

The neuromodulation controller

The neuromodulation controller adjusts a subset of n conductances, denoted as $\bar{g}_{\text{mod}} \in \mathbb{R}^n$ with $n < N$, using the algorithm introduced in [30]. This controller employs the concept of Dynamic Input Conductances (DICs) to determine target values for $\bar{g}_{\text{mod}}$ based on the input neuromodulator concentration, represented as $\bar{g}_0\left([\text{nmod}]\right) \in \mathbb{R}^n$. The error between the target and the current values, e_{mod}, drives a Proportional-Integral (PI) controller, which updates $\bar{g}_{\text{mod}}$ to track the desired reference.

The controller dynamics are described by the following equations:

$$
\begin{aligned}
e_{\mathrm{mod}} &= \bar{g}_0\left([\mathrm{nmod}]\right) - \bar{g}_{\mathrm{mod}}, \\
\dot{\bar{g}}_{\mathrm{mod}} &= f\left(K_p \cdot e_{\mathrm{mod}} + K_i \cdot \int e_{\mathrm{mod}} \mathrm{d}t\right),
\end{aligned}
$$

where K_p and K_i are the proportional and integral gains of the PI controller, respectively. In summary, the controller adjusts the modulated conductances $\bar{g}_{\mathrm{mod}}$ in response to the local concentration of neuromodulator, producing new reference values for these conductances to fine-tune the cell firing pattern – effectively neuromodulating it. This neuromodulator controller produces changes in conductance ratios that are normally preserved within the homeostatic controller. The new reference values depend on the neuromodulator concentration, the type of neuron, and the cell's current state, characterized by the full set of conductances $\bar{g}_{\mathrm{ion}} \in \mathbb{R}^N$. The computation of these references is achieved through DICs, which encapsulate this complexity.

DICs consist of three voltage-dependent conductances that separate according to timescales: one fast, one slow, and one ultraslow, denoted as $g_{\mathrm{f}}(V)$, $g_{\mathrm{s}}(V)$, and $g_{\mathrm{u}}(V)$, which can be computed as linear functions of the maximal conductance vector $\bar{g}_{\mathrm{ion}} \in \mathbb{R}^N$ of an N-channel conductance-based model at each voltage level V:

$$
[g_{\mathrm{f}}(V); g_{\mathrm{s}}(V); g_{\mathrm{u}}(V)] = f_{\mathrm{DIC}}(V) = S(V) \cdot \bar{g}_{\mathrm{ion}}\,,
$$

where $S(V) \in \mathbb{R}^{3\times N}$ is a sensitivity matrix that can be built by: $S_{i\,j}(V) = -\left(w_{i\,j} \cdot \frac{\partial \dot{V}}{\partial X_j} \frac{\partial X_{j,\infty}}{\partial V}\right) / g_{\mathrm{leak}}$, where i denotes the timescale, X_j are gating variables of the j-th channel of the considered model and $w_{i\,j}$ is a timescale-dependent weight which is computed as the logarithmic distance of the time constant of X_j and the timescale i [54]. While the complete curve of the DICs may be of interest, only its value at the threshold voltage V_{th} is used, as the values and signs of the DICs at V_{th} reliably determine the firing pattern [54, 55]. Thus, the following linear system $f_{\mathrm{DIC}}(V_{\mathrm{th}}) = S(V_{\mathrm{th}}) \cdot \bar{g}_{\mathrm{ion}}$ makes the link between ion channel conductances and neuronal activity.

Use of generative AI

The ChatGPT-5 chatbot has been used to improve the syntax and grammar of several paragraphs in the manuscript. After using this tool/service, the authors reviewed and edited the content as needed and take full responsibility for the content of the published article.

Supporting information

S1 Appendix Details and additional experiments We provide all the elements required to reproduce the results presented in this paper, as well as additional experiments and their results. This includes, for example, model equations and their parameter values.

References

1. Bargmann CI, Marder E. From the connectome to brain function. Nat Methods. 2013;10(6):483-90. doi:10.1038/nmeth.2451.
2. Marder E, O'Leary T, Shruti S. Neuromodulation of circuits with variable parameters: single neurons and small circuits reveal principles of state-dependent and robust neuromodulation. Annu Rev Neurosci. 2014;37:329-46. doi:10.1146/annurev-neuro-071013-013958.
3. Marder E, Calabrese RL. Principles of rhythmic motor pattern generation. Physiol Rev. 1996;76(3):687-717. doi:10.1152/physrev.1996.76.3.687.
4. Marder E, Bucher D. Central pattern generators and the control of rhythmic movements. Curr Biol. 2001;11(23):R986-96. doi:10.1016/S0960-9822(01)00581-4.
5. McCormick DA, Nestvogel DB, He BJ. Neuromodulation of brain state and behavior. Annu Rev Neurosci. 2020;43:391-415. doi:10.1146/annurev-neuro-100219-105424.
6. Nadim F, Bucher D. Neuromodulation of neurons and synapses. Curr Opin Neurobiol. 2014;29:48-56. doi:10.1016/j.conb.2014.05.003.

7. Hooper SL, Marder E. Modulation of a central pattern generator by two neuropeptides, proctolin and FMRFamide. Brain Res. 1984;305(1):186-91. doi:10.1016/0006-8993(84)91138-7.

8. Desai NS. Homeostatic plasticity in the CNS: synaptic and intrinsic forms. J Physiol Paris. 2003;97(4-6):391-402. doi:10.1016/j.jphysparis.2004.01.005.

9. Marder E, Goaillard JM. Variability, compensation and homeostasis in neuron and network function. Nat Rev Neurosci. 2006;7(7):563-74. doi:10.1038/nrn1949.

10. O'Leary T, Williams AH, Caplan JS, Marder E. Correlations in ion channel expression emerge from homeostatic tuning rules. Proc Natl Acad Sci U S A. 2013;110(28):E2645-54. doi:10.1073/pnas.1309966110.

11. Davis GW. Homeostatic signaling and the stabilization of neural function. Neuron. 2013;80(3):718-28. doi:10.1016/j.neuron.2013.09.044.

12. Turrigiano GG. Homeostatic plasticity in neuronal networks: The more things change, the more they stay the same. Trends Neurosci. 1999;22(5):221-7. doi:10.1016/S0166-2236(98)01341-1.

13. Turrigiano GG, Nelson SB. Homeostatic plasticity in the developing nervous system. Nat Rev Neurosci. 2004;5(2):97-107. doi:10.1038/nrn1327.

14. Turrigiano G. Homeostatic synaptic plasticity: Local and global mechanisms for stabilizing neuronal function. Cold Spring Harb Perspect Biol. 2012;4(1):a005736. doi:10.1101/cshperspect.a005736.

15. Marder E. Variability, compensation, and modulation in neurons and circuits. Proc Natl Acad Sci U S A. 2011;108(supplement_3):15542-8. doi:10.1073/pnas.1010674108.

16. O'Leary T, Wyllie DJ. Neuronal homeostasis: time for a change? J Physiol. 2011;589(20):4811-26. doi:10.1113/jphysiol.2011.210179.

17. Marder E, Prinz AA. Modeling stability in neuron and network function: the role of activity in homeostasis. Bioessays. 2002;24(12):1145-54. doi:10.1002/bies.10185.

18. O'Leary T, van Rossum MC, Wyllie DJ. Homeostasis of intrinsic excitability in hippocampal neurones: dynamics and mechanism of the response to chronic depolarization. J Physiol. 2010;588(1):157-70. doi:10.1113/jphysiol.2009.181024.

19. Pratt KG, Aizenman CD. Homeostatic regulation of intrinsic excitability and synaptic transmission in a developing visual circuit. J Neurosci. 2007;27(31):8268-77. doi:10.1523/jneurosci.1738-07.2007.

20. Izhikevich EM. Dynamical Systems in Neuroscience: The Geometry of Excitability and Bursting. 1st ed. Cambridge, MA: MIT Press; 2007. doi:10.7551/mitpress/2526.001.0001.

21. Hodgkin AL, Huxley AF. A quantitative description of membrane current and its application to conduction and excitation in nerve. J Physiol. 1952;117(4):500-44. doi:10.1113/jphysiol.1952.sp004764.

22. Liu Z, Golowasch J, Marder E, Abbott L. A model neuron with activity-dependent conductances regulated by multiple calcium sensors. J Neurosci. 1998;18(7):2309-20. doi:10.1523/JNEUROSCI.18-07-02309.1998.

23. Qian K, Yu N, Tucker KR, Levitan ES, Canavier CC. Mathematical analysis of depolarization block mediated by slow inactivation of fast sodium channels in midbrain dopamine neurons. J Neurophysiol. 2014;112(11):2779-90. doi:10.1152/jn.00578.2014.

24. Plant RE. Bifurcation and resonance in a model for bursting nerve cells. J Math Biol. 1981;11:15-32. doi:10.1007/bf00275821.

25. Wechselberger M, Wright CL, Bishop GA, Boulant JA. Ionic channels and conductance-based models for hypothalamic neuronal thermosensitivity. Am J Physiol Regul Integr Comp Physiol. 2006;291(3):R518-29. doi:10.1152/ajpregu.00039.2006.

26. Drion G, Massotte L, Sepulchre R, Seutin V. How modeling can reconcile apparently discrepant experimental results: the case of pacemaking in dopaminergic neurons. PLOS Comput Biol. 2011;7(5):e1002050. doi:10.1371/journal.pcbi.1002050.

27. Katori Y, Lang EJ, Onizuka M, Kawato M, Aihara K. Quantitative modeling of spatio-temporal dynamics of inferior olive neurons with a simple conductance-based model. Int J Bifurcat Chaos. 2010;20(3):583-603. doi:10.1142/s0218127410025909.

28. Megwa OF, Pascual LM, Günay C, Pulver SR, Prinz AA. Temporal dynamics of Na/K pump mediated memory traces: insights from conductance-based models of Drosophila neurons. Front Neurosci. 2023;17:1154549. doi:10.1101/2023.03.07.531036.

29. O'Leary T, Williams AH, Franci A, Marder E. Cell types, network homeostasis, and pathological compensation from a biologically plausible ion channel expression model. Neuron. 2014;82(4):809-21. doi:10.1016/j.neuron.2014.04.002.

30. Fyon A, Sacré P, Franci A, Drion G. Reliable neuromodulation from adaptive control of ion channel expression. IFAC-PapersOnLine. 2023;56(2):458-63. doi:10.1016/j.ifacol.2023.10.1610.

31. Goaillard JM, Marder E. Ion channel degeneracy, variability, and covariation in neuron and circuit resilience. Annu Rev Neurosci. 2021;44:335-57. doi:10.1146/annurev-neuro-092920-121538.

32. Fyon A, Franci A, Sacré P, Drion G. Dimensionality reduction of neuronal degeneracy reveals two interfering physiological mechanisms. PNAS Nexus. 2024;3(10):pgae415. doi:10.1093/pnasnexus/pgae415.

33. Yuste R, MacLean JN, Smith J, Lansner A. The cortex as a central pattern generator. Nat Rev Neurosci. 2005;6(6):477-83. doi:10.1038/nrn1686.

34. Guertin PA. The mammalian central pattern generator for locomotion. Brain Res Rev. 2009;62(1):45-56. doi:10.1016/j.brainresrev.2009.08.002.

35. Gutierrez GJ, O'Leary T, Marder E. Multiple mechanisms switch an electrically coupled, synaptically inhibited neuron between competing rhythmic oscillators. Neuron. 2013;77(5):845-58. doi:10.1016/j.neuron.2013.01.016.

36. Drion G, Franci A, Sepulchre R. Cellular switches orchestrate rhythmic circuits. Biol Cybern. 2019;113:71-82. doi:10.1007/s00422-018-0778-6.

37. Selverston A, Szücs A, Huerta R, Pinto RD, Reyes MB. Neural mechanisms underlying the generation of the lobster gastric mill motor pattern. Front Neural Circuits. 2009;3:608. doi:10.3389/neuro.04.012.2009.

38. Cunha R. Adenosine as a neuromodulator and as a homeostatic regulator in the nervous system: Different roles, different sources and different receptors. Neurochem Int. 2001;38(2):107-25. doi:10.1016/s0197-0186(00)00034-6.

39. Kramer RH, Levitan IB. Activity-dependent neuromodulation in Aplysia neuron R15: intracellular calcium antagonizes neurotransmitter responses mediated by cAMP. J Neurophysiol. 1990;63(5):1075-88. doi:10.1152/jn.1990.63.5.1075.

40. Raymond JL, Baxter DA, Buonomano DV, Byrne JH. A learning rule based on empirically-derived activity-dependent neuromodulation supports operant conditioning in a small network. Neural Netw. 1992;5(5):789-803. doi:10.1016/s0893-6080(05)80140-6.

41. Marcus DJ, Bruchas MR. Optical approaches for investigating neuromodulation and G protein–coupled receptor signaling. Pharmacol Rev. 2023;75(6):1119-39. doi:10.1124/pharmrev.122.000584.

42. Scheler G. Regulation of neuromodulator receptor efficacy—implications for whole-neuron and synaptic plasticity. Prog Neurobiol. 2004;72(6):399-415. doi:10.1016/s0301-0082(04)00045-0.

43. Starmer CF, Lastra AA, Nesterenko VV, Grant AO. Proarrhythmic response to sodium channel blockade. Theoretical model and numerical experiments. Circulation. 1991;84(3):1364-77. doi:10.1161/01.cir.84.3.1364.

44. Grant A, Starmer C, Strauss H. Antiarrhythmic drug action. Blockade of the inward sodium current. Circ Res. 1984;55(4):427-39. doi:10.1161/01.res.55.4.427.

45. Anger T, Madge DJ, Mulla M, Riddall D. Medicinal chemistry of neuronal voltage-gated sodium channel blockers. J Med Chem. 2001;44(2):115-37. doi:10.1021/jm000155h.

46. Whitacre JM. Degeneracy: A link between evolvability, robustness and complexity in biological systems. Theor Biol Med Model. 2010;7:1-17. doi:10.1186/1742-4682-7-6.

47. Rathour RK, Narayanan R. Degeneracy in hippocampal physiology and plasticity. Hippocampus. 2019;29(10):980-1022. doi:10.1101/203943.

48. Whitacre J, Bender A. Degeneracy: A design principle for achieving robustness and evolvability. J Theor Biol. 2010;263(1):143-53. doi:10.1016/j.jtbi.2009.11.008.

49. Prinz AA. Degeneracy rules! J Physiol. 2017;595(8):2409. doi:10.1113/jp273924.

50. Cubeddu L. Drug-induced inhibition and trafficking disruption of ion channels: Pathogenesis of QT abnormalities and drug-induced fatal arrhythmias. Curr Cardiol Rev. 2016;12(2):141-54. doi:10.2174/1573403x12666160301120217.

51. DeWitt CR, Waksman JC. Pharmacology, pathophysiology and management of calcium channel blocker and β-blocker toxicity. Toxicol Rev. 2004;23:223-38. doi:10.2165/00139709-200423040-00003.

52. Imbrici P, Nicolotti O, Leonetti F, Conte D, Liantonio A. Ion channels in drug discovery and safety pharmacology. In: Computational Toxicology: Methods and Protocols. vol. 1800. Springer; 2018. p. 313-26. doi:10.1007/978-1-4939-7899-1_15.

53. Bezanson J, Edelman A, Karpinski S, Shah VB. Julia: A fresh approach to numerical computing. SIAM Rev. 2017;59(1):65-98. doi:10.1137/141000671.

54. Drion G, Franci A, Dethier J, Sepulchre R. Dynamic input conductances shape neuronal spiking. eNeuro. 2015;2(1). doi:10.1523/ENEURO.0031-14.2015.

55. Brandoit J, Ernst D, Drion G, Fyon A. Fast reconstruction of degenerate populations of conductance-based neuron models from spike times [Preprint]. arXiv:2509.12783; 2025 [cited 2025 December 05]. Available from: `https://arxiv.org/abs/2509.12783`.